Collisional Relaxation of the Three Vibrationally Excited Difluorobenzene Isomers by Collisions with CO_2: Effect of Donor Vibrational Mode

Deborah G. Mitchell, Alan M. Johnson, Jeremy A. Johnson,† Kortney A. Judd, Kilyoung Kim, Maurine Mayhew, Amber L. Powell, and Eric T. Sevy*

Department of Chemistry and Biochemistry, Brigham Young University, Provo, Utah 84602

Received: September 5, 2007; In Final Form: October 17, 2007

Relaxation of highly vibrationally excited 1,2-, 1,3-, and 1,4-difluorobenzne (DFB) by collisions with carbon dioxide has been investigated using diode laser transient absorption spectroscopy. Vibrationally hot DFB ($E' \approx 41\,000$ cm^{-1}) was prepared by 248 nm excimer laser excitation followed by rapid radiationless relaxation to the ground electronic state. Collisions between hot DFB isomers and CO_2 result in large amounts of rotational and translational energy transfer from the hot donors to the bath. The CO_2 nascent rotational population distribution of the high-J ($J = 58-80$) tail of the 00^00 state was probed at short times following the excimer laser pulse to measure rate constants and probabilities for collisions populating these states. The amount of translational energy gained by CO_2 during collisions was determined using Doppler spectroscopy to measure the width of the absorption line for each transition. The energy transfer probability distribution function, $P(E,E')$, for the large ΔE tail was obtained by resorting the state-indexed energy transfer probabilities as a function of ΔE. $P(E,E')$ was fit to a biexponential function to determine the average energy transferred in a single DFB/CO_2 collision and fit parameters describing the shape of $P(E,E')$. $P(E,E')$ fit parameters for DFB/CO_2 and the previously studied C_6F_6/CO_2 system are compared to various donor molecular properties. A model based on Fermi's Golden Rule indicates that the shape of $P(E,E')$ is primarily determined by the low-frequency out-of-plane donor vibrational modes. A fractional mode population analysis is performed, which suggests that for energy transfer from DFB and C_6F_6 to CO_2 the two key donor vibrational modes from which energy leaks out of the donor into the bath are ν_{11} and ν_{16}. These "gateway" modes are some of the same modes determined to be the most efficient energy transfer modes by quantum scattering studies of benzene/He collisions.

I. Introduction

Collisional processes in which energy is transferred between molecules play an important role in a wide range of systems including chemical lasers, atmospheric processes, and combustion chemistry.[1] Of particular importance in understanding the fate of molecules with large amounts of energy during collision events is the energy transfer probability distribution function, $P(E,E')$, which describes the probability that a molecule initially possessing energy E' will have energy E after a collision.[2] Despite many years of interest in energy transfer in general and in P(E,E') in particular, it has only been in the last 10 years that this function has been measured experimentally.[3−5]

Recent efforts in our lab have used the diode probe technique developed by Flynn and co-workers[6−8] to experimentally measure $P(E,E')$ for the relaxation of vibrationally excited pyrimidine[9] and pyridine[10] via collisions with a carbon dioxide bath. The particular focus of our efforts has been to understand the relationship between the shape and the magnitude of $P(E,E')$ and the molecular properties of the donor molecules involved in the energy transfer process. In all systems studied to date with a donor energy of $E' \approx 41\,000$ cm^{-1}, when the constraints of normalization and detailed balance are considered, $P(E,E')$ cannot be described by a single-exponential function. Experimentally obtained $P(E,E')$ values have been fit to a biexponential model function, which is described by three parameters: one describing the shape of the strong collision tail (large ΔE), one describing the shape of the weak collision region (small ΔE), and one giving the relative contributions of the two different exponential functions. An application of Fermi's Golden Rule indicates that the shape of $P(E,E')$, as determined by the biexponential fit parameters, is correlated with the how the donor molecule density of states changes with internal energy. This application of Fermi's Golden Rule is proving to be a potentially useful predictor for the shape of $P(E,E')$ describing collisional energy transfer from many different aromatic donor molecules to CO_2[9−13] and H_2O.[14]

We previously reported[8−10] a "fractional energy transfer distribution", $f(E,E')$, model, which has been successful in understanding the shape of $P(E,E')$. This model takes into account both the efficiency with which a donor vibrational mode can impart energy in collisions as well as the ability of the mode to transfer that amount of energy, as determined by the fraction of donor molecules with sufficient energy in the mode to transfer a given ΔE. Use of this model indicates that the shape of $f(E,E')$ most closely mirrors the shape of the experimentally obtained $P(E,E')$ when energy is assumed to leak out of only low-frequency modes into the bath. These findings are consistent with quantum scattering[15] calculations, which observe that only a few vibrational modes (those with lower-frequency and out-of-plane-type motion) have significant energy transfer cross-

* Author to whom correspondence should be addressed. Phone: (801) 422-7235. Fax: (801) 422-0153. E-mail: esevy@byu.edu.

† Present address: Department of Chemistry, Massachusetts Institute of Technology, Cambridge, MA 02139.

10.1021/jp0771365 CCC: $40.75
Published on Web 01/18/2008

sections in studies of energy transfer from benzene to He. Lendvay,[16] in classical trajectory studies of relaxation of CS_2, has also noted that only certain vibrational modes are effective at transferring energy during collisions. He has referred to these effective modes as "gateway" modes, or "conduits", for energy transfer.

Previous studies have linked other donor molecule properties to parameters that describe $P(E,E')$. Comparison of the pyridine[10] and pyrimidine[9] results to those of pyrazine,[3,6] C_6F_6,[3,7] and methylpyrazine[8] suggest that the strong collision exponent contributes more to the shape of $P(E,E')$ when the donor molecule has a large number of low-frequency donor modes. C_6F_6, with the most low-frequency modes, has the largest "fraction" of strong collisions. Alternatively, results from these comparisons also suggest that the strong collision exponent contributes the least (i.e., the fraction of strong collisions is the smallest) when the donor molecule has a large dipole moment. Mullin and co-workers[17] have shown that pyridine, which has a large dipole moment, has an increased ratio of $V \rightarrow V$ versus $V \rightarrow RT$ energy transfer probability when compared to that of pyrazine, which has no dipole. Our studies of pyridine[10] energy transfer indicate that $P(E,E')$ for pyridine has the smallest "fraction" of strong collisions. We attributed this to pyridine's large dipole moment, which led to enhanced $V \rightarrow V$ energy transfer probability.

These studies represent the continued efforts in our laboratory to understand $P(E,E')$ and the donor molecular properties that govern its shape. Here we present a study of the collisional relaxation of the three difluorobenzene (DFB) isomers, 1,2-difluorobenzene, 1,3-difluorobenzene, and 1,4-difluorobenzene. These three donors all have the same number vibrational modes, each with the same motion, which are also the same as C_6F_6. However, the frequencies of some of the modes are different, depending on the position of the fluorine atoms. The results of these studies will allow us to directly compare vibrational modes between different donors and gain greater understanding of the relationship between donor mode character and frequency with $P(E,E')$. These three donors also have different dipole moments, which will allow us to test the potential relationship between dipole moment and the biexponential fit parameters that describe $P(E,E')$.

II. Experimental Section

The UV pump/IR probe technique used to study the collisional relaxation of the three isomers of difluorobenzene has been described in detail elsewhere;[9] therefore, only a brief outline of the method is presented here. A 1:1 mixture of gas-phase difluorobenzene and CO_2 flows through a 3.0 m Pyrex collision cell at a total pressure of 20 mTorr. A 248 nm KrF excimer laser (Lamda Physik Complex 201) is used to excite the $S_1 \leftarrow S_0$ transition of difluorobenzene.[18−20] Electrically excited difluorobenzene then undergoes a rapid radiationless internal conversion into highly vibrationally excited states in the ground electronic state, $S_0^* \leftarrow S_1$.[20−22] Energy gain into individual rotational states of the CO_2 (00^00) vibrational state resulting from collisions with hot difluorobenzene in S_0^* is monitored by probing the transient absorption of IR light ($\lambda = 4.3\ \mu$m) that is collinearly propagated with the UV beam through the collision cell. The highly resolved (0.0003 cm^{-1}) IR laser (Laser Components) is used to probe the scattered CO_2 molecules via the antisymmetric stretch transition of CO_2. To ensure that only a single diode laser mode is detected, the infrared light is passed through a single grating monochromator (Acton Spectra pro 500i) before being focused onto a liquid nitrogen cooled InSb detector (Judson Technologies). The detector and preamplifier (Perry Amplifier) combination has a rise time of approximately 400 ns, shorter than $^1/_4$ of the gas kinetic collision time (1 μs). The signal from the InSb detector is digitized and stored on a LeCroy LT342 Waverunner digital oscilloscope before being transferred to a computer for further analysis. Approximately 4% of the infrared light is split off and passed through a reference line. The reference beam passes through a monochromator and is focused onto a high-gain InSb detector (Judson Technologies). The output of the reference detector is used as input to a lock-in amplifier (Stanford Research Systems). The lock-in amplifier generates an error signal that is fed back to the diode laser control electronics, allowing active stabilization of the laser frequency.

Determination of rovibrational state populations requires a measurement of both the transient absorption at the center of the line and the Doppler broadened line shape; therefore, two types of measurements are collected for each rotational state: the transient fractional absorption, $\Delta I/I$, after 1 μs ($^1/_4$ of the gas kinetic collision time of 4 μs) at the center frequency of the transition and a measure of the Doppler broadened full width at half-maximum (fwhm). The center line measurement is obtained by locking the diode laser frequency to the appropriate CO_2 line and averaging the absorption over approximately 100 excimer laser shots. A dual-channel technique[6,9] is employed to account for short-term fluctuations in the diode laser intensity, while a reference line scheme[23] is used with the center line measurements to correct for longer-term drifts in the system. An additional short-cell and long-cell reference procedure[9] is performed to determine the absolute scattering rate constant and to calibrate the measured probabilities to previously measured systems. Line shape measurements are performed by locking the diode laser frequency to the peak of a scanning Fabry−Perot Etalon fringe (free spectral range = 289 MHz). Absorption by CO_2 is then measured at a series of 30−40 frequencies distributed evenly over the line shape, averaged over 100 excimer laser shots at each frequency.

1,2-Diflurobenzene (Aldrich, 98% purity), 1,3-difluorobenzene (Aldrich 99% purity), and 1,4 difluorobenzene (99% purity) were purified prior to our experiments using the freeze−pump−thaw method, while research-grade CO_2 (Intermountain Airgas, Inc., 99.999%) was used without further purification.

III. Results

A. Rotational and Translational Excitation of the Carbon Dioxide Bath. Transient CO_2 populations in various J states of the ground vibrational level, ranging from $J = 58$ to $J = 80$, were monitored via infrared absorption following UV excitation of 1,2-, 1,3-, and 1,4-DFB at 248 nm. Because the CO_2 rotational[24−29] and translational[30] energies change with each collision, the distributions probed at short times after the excimer laser pulse represent the nascent collision dynamics without significant relaxation. Typical transient signals for the three systems are shown in Figure 1, where absorption on the CO_2 (00^00, $J = 70$) $\rightarrow$ CO_2 (00^01, $J = 69$) line at 2279.8391 cm^{-1} is plotted versus time relative to the excimer laser pulse. Each transient absorption is averaged over 100 excimer laser shots fired into a flowing gas mixture of 10 mTorr CO_2 and 10 mTorr 1,2-DFB (lower curve), 1,3-DFB (middle curve), and 1,4-DFB (upper curve). The early rise in the signal represents predominantly single-collision excitation of CO_2 to $J = 70$ by collisions with vibrationally hot DFB. The time dependence of the signal at longer times ($t > 4\ \mu$s) is dictated by the competition between the continued filling of this state by CO_2 colliding with slightly

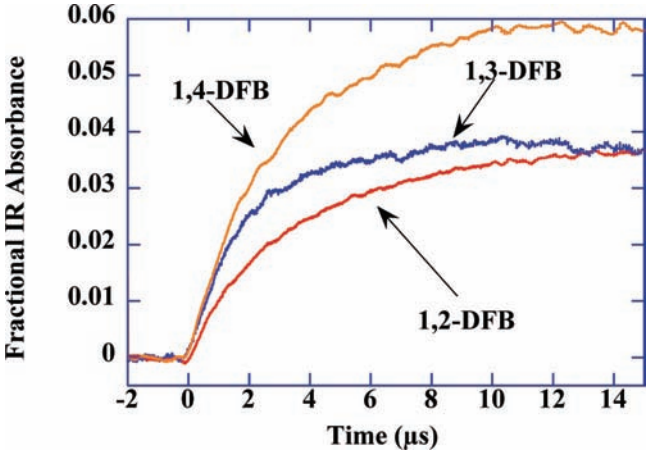

Figure 1. Fractional IR absorption of CO_2 collisionally scattered into the 00^00, $J = 70$ state as a function of time following UV excitation of the three isomers of DFB. Transient signals were obtained using a flowing gas mixture of 10 mTorr CO_2 and 10 mTorr of 1,2-DFB (lower curve), 1,3-DFB (middle curve), or 1,4-DFB (upper curve) with a mean kinetic collision time of 4 μs. The transient signal indicates that more molecules are scattered into the CO_2 (00^00, $J = 70$) state by collisions with 1,4-DFB followed by 1,3- and 1,2-DFB on the same time scale; thus the scattering rate constant and probability for this state will be greater for collisions with 1,4-DFB.

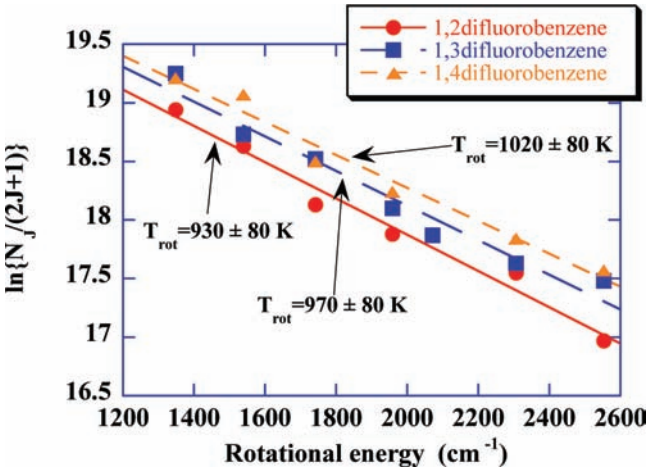

Figure 2. Boltzmann plot of the nascent rotational distributions in the ground vibrational level of CO_2 following excitation by collisions with vibrationally hot 1,2-, 1,3-, and 1,4-DFB. The solid lines are the best linear least-squares fit to the experimental points measured over the range $J = 58-80$. The slope of the best-fit line is equal to $-1/k_B T_{rot}$, and the number densities, $N(J)$, are in units of molecules/cm^3. The rotational temperatures for CO_2 molecules scattered into the high-J states following collisions with 1,2-, 1,3-, and 1,4-DFB are 930, 970, and 1020 $\pm$ 80 K, respectively.

thermalized DFB molecules and CO_2 rotational relaxation out of this high angular momentum state. Although the absorption signal is a measure of the change in the population difference between the initial and the final states of the probe transition, earlier pyrazine/CO_2[31] and C_6F_6/CO_2[32] experiments show that the number of molecules scattered into the high-J tail of the 00^01 state is insignificant. Thus, the measured absorptions reflect a transient increase in the population of molecules in the high-J tail of the ground vibrational level. The greater absorption signal for collisions between 1,4-DFB and CO_2 indicate that a greater number of bath molecules are scattered into $J = 70$ in these collisions than in collisions with the other two DFB molecules. This results in a larger scattering rate constant and probability, given a constant excited DFB concentration for all three systems. Conversion of the measured absorptions to CO_2 number density is straightforward[33] given the absorption line strengths taken from the HITRAN spectroscopic database.[34]

The rotational distributions over the final range of J states studied here are well-described by a rotational temperature. A Boltzmann plot of the rotational distribution created by collisions of CO_2 with the three DFB isomers is shown in Figure 2. For each system it is important to realize that the determined rotational temperature only describes the high-J tail ($J = 58-80$) of the rotational distribution and may not accurately describe molecules scattering into lower-J states. In fact, there is no reason to expect that a temperature will provide a suitable description of any part of the rotational distribution created by collisions with a vibrationally hot molecule; however, given that a single temperature does characterize these high-J CO_2 (00^00) states, the temperature can be viewed as a convenient measure of the amount of rotational excitation. The measured rotational temperatures, 930, 970, and 1020 $\pm$ 80 K for 1,2-, 1,3-, and 1,4-DFB, respectively, indicate that CO_2 molecules are scattered into the high-J states during the collision process and that a large amount of energy is transferred from vibrationally excited DFB to CO_2 in a single collision. These rotational temperatures are comparable to those obtained in other energy transfer studies involving highly vibrationally excited molecules and CO_2 (methylpyrazine,[8] 725 K; C_6F_6,[7] 795 K; pyridine,[10] 1040 K; pyrazine,[6] 1300 K; pyrimidine,[9] 1660 K).

The projections of the distributions of CO_2 lab frame, recoil velocities onto the probe beam axis were determined by measuring the Doppler broadened line shapes of the probe transitions. As seen in Figure 3, a Gaussian function accurately fits the measured line shapes for CO_2 following collisions with each of the three DFB isomers, indicating that a single translational temperature can suitably describe the CO_2 translational excitation. Figure 3a shows the transient absorption line shape obtained from a measurement taken 1 μs after excimer laser excitation of a mixture of 10 mTorr of 1,2-DFB and 10 mTorr of CO_2, while Figures 3b and 3c show the transient line shape taken 1 μs after excimer laser excitation of a mixture of 10 mTorr of 1,3- and 1,4-DFB and 10 mTorr of CO_2. The line widths (fwhm) obtained from probing CO_2 scattered into $J = 70$ are $\Delta\nu = 0.0103$, 0.0101, and 0.0104 $\pm$ 0.0005 cm^{-1} for collisions with 1,2-, 1,3-, and 1,4-DFB, respectively. For comparison purposes, the line width of a transition probing CO_2 molecules with a room-temperature velocity distribution is $\Delta\nu = 0.0042$ cm^{-1}. Because postcollision velocity distributions are isotropic,[6] the measured translational temperatures describe the three-dimensional speed distribution of the CO_2 molecules following collisions with highly vibrationally excited DFB.

Full width at half-maximum Doppler line widths for the absorption transitions probing scattering into J states between 58 and 80 are given in Table 1 along with the corresponding lab frame translational temperatures and DFB/CO_2 relative (center of mass) temperatures, which are necessary to determine the actual energy transfer in these collisions. Three notable features of the line width data in Table 1 and shown graphically in Figure 4 should be highlighted. First, the broadened line widths indicate that collisions scattering molecules into high CO_2 rotational states produce broad (high-temperature) velocity distributions, indicating that these collisions are accompanied by large translational energy transfers. Second, the line widths vary linearly with the final rotational angular momentum, indicating that the DFB/CO_2 impact parameter for these collisions is nearly constant over this range of final J states.[8]

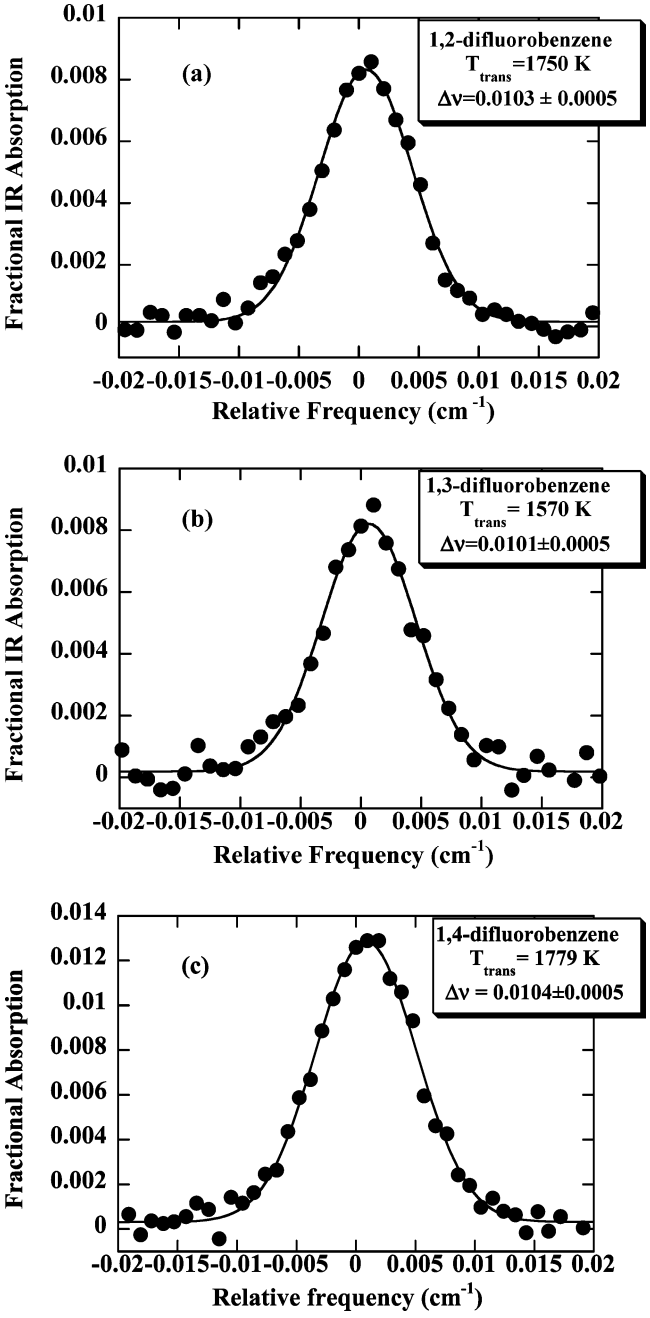

Figure 3. Nascent Doppler broadened line shapes for the absorption transition CO_2 (00^00; $J = 70$) → CO_2 (00^01; $J = 69$) probing CO_2 molecules excited by collisions with vibrationally excited (a) 1,2-, (b) 1,3-, and (c) 1,4-DFB. The line shapes were obtained using a flowing mixture of 10 mTorr CO_2 and 10 mTorr DFB. The points represent the fractional IR absorption of CO_2 collisionally scattered into the 00^00, $J = 70$ state measured 1 μs following 248 nm excimer laser pumping of DFB. Absorption measurements are averaged over approximately 100 excimer laser shots fired at 1 Hz at each frequency across the line. The solid lines are the best nonlinear least-squares fit to a Gaussian function. The line widths obtained from the measured line shapes are 0.0103, 0.0100, and 0.0104 ± 0.0005 for 1,2-, 1,3-, and 1,4-DFB, respectively. For comparison, the fwhm of a CO_2 line shape with T_{trans} = 300 K is approximately 0.0042 cm^{-1}.

Finally, the line widths (and the associated translational temperatures) for CO_2 following collisions with 1,4-DFB increase with J more than the CO_2 line widths following collisions with the other two isomers, while collisions with 1,2-DFB produce the least increase in CO_2 line widths as a function of final CO_2 rotational state.

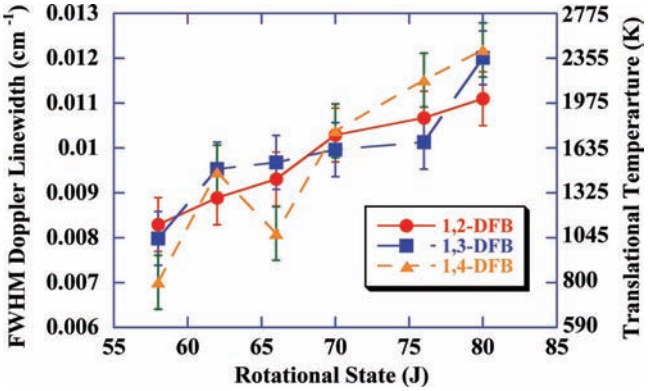

Figure 4. Full width at half-maximum Doppler line widths of absorption transitions probing high rotational states of CO_2 following collisions with vibrationally hot DFB plotted versus the final rotational state J. The lab frame translational temperatures determined from the measured line widths are given on the right y-axis. The line widths are measured 1 μs following 248 nm excimer laser excitation of the DFB, ensuring that the measured velocity distributions are nascent ($\tau_{coll} \approx 4$ μs). The fwhm appropriate for a 298 K velocity distribution is 0.0042 cm^{-1}.

B. Final State-Resolved Energy Transfer Rate Constants and Probabilities. At times much less than the mean gas kinetic collision time, the state-specific rate constant, k_2^J, for excitation of CO_2 from a thermal distribution into state J can be obtained from the expression

$$k_2^J = \frac{[CO_2(00^00,J,V)]}{[CO_2]_0[DFB^{E'}]_0 t} \quad (1)$$

where $[CO_2]_0$ is the bulk carbon dioxide number density, $[DFB^{E'}]_0$ is the number density of difluorobenzene molecules excited by the excimer laser pulse to an energy E', determined from the UV absorption, and $[CO_2(00^00,J,V)]$ is the state-specific CO_2 concentration obtained from infrared absorption measurements.

The absolute rate constants for excitation of CO_2 into the high-J tail of the ground vibrational level by collisions with hot DFB ($E' \approx 40\,000$ cm^{-1}) are given in Table 2. As noted in the experimental description, these rate constants are scaled both on an absolute scale as well as to previous pyrazine/CO_2 scattering studies.[6] Table 2 also includes the Lennard-Jones scattering probabilities for excitation of each final rotational state. The probability that a CO_2 molecule is scattered into a particular final J state is defined as the energy transfer rate constant, k_2^J, divided by the Lennard-Jones collision rate constant

$$\text{Prob}^J = \frac{k_2^J}{k_{LJ}} \quad (2)$$

The choice of the Lennard-Jones collision rate constants to determine the energy transfer probability has been discussed elsewhere[9] and is used in these studies so that results can be directly compared to previously studied systems.

C. Energy Transfer Probability Distribution Function. The energy transfer probability distribution function, $P(E,E')$, for the large ΔE region can be obtained from state-resolved data reported here.[3] The conversion of quantum state-resolved probabilities to $P(E,E')$ requires knowledge of both the initial and the final CO_2 rotational state. Final J states are well-defined in these studies; however, initial states can only be described

TABLE 1: Full Width at Half-Maximum Doppler Line Widths,[a] Translational Temperatures,[b] and Center of Mass Translational Temperatures[c] for $CO_2(00^00, J)$ Following Collisions with Highly Vibrationally Excited 1,2-Difluorobenzene[E′], 1,3-Difluorobenzene[E′], and 1,4-Difluorobenzene[E′d]

	1,2-difluorobenzene			1,3-difluorobenzene			1,4-difluorobenzene		
CO_2[e] $(00^00,J)$	$\Delta\nu_{obs}$[a] (cm^{-1})	T_{trans}[b] (K)	T_{trans}^{COM}[c] (K)	$\Delta\nu_{obs}$[a] (cm^{-1})	T_{trans}[b] (K)	T_{trans}^{COM}[c] (K)	$\Delta\nu_{obs}$[a] (cm^{-1})	T_{trans}[b] (K)	T_{trans}^{COM}[c] (K)
58	0.0083 ± 0.0006	1120± 160	1440 ± 230	0.0080 ± 0.0006	1030 ± 160	1310 ± 220	0.0070 ± 0.0006	800 ± 140	990 ± 440
62	0.0089 ± 0.0006	1290 ± 180	1680 ± 240	0.0095 ± 0.0006	1280 ± 210	1660 ± 280	0.0095 ± 0.0006	1470 ± 200	1920 ± 270
66	0.0093 ± 0.0005	1420 ± 150	1860 ± 210	0.0097 ± 0.0005	1420 ± 160	1850 ± 220	0.0081 ± 0.0006	1080 ± 170	1380 ± 470
70	0.0103 ± 0.0005	1750 ± 170	2310 ± 240	0.0100 ± 0.0005	1570 ± 170	2060 ± 230	0.010 ± 0.0005	1780 ± 180	2350 ± 240
72				0.0109 ± 0.0005	1960 ± 180	2590 ± 250			
76	0.0107 ± 0.0005	1890 ± 180	2500 ± 250	0.0101 ± 0.0005	1710 ± 170	2250 ± 230	0.0115 ± 0.0005	2200 ± 190	2940 ± 430
80	0.0111 ± 0.0005	2050 ± 190	2730 ± 260	0.0120 ± 0.0005	2400 ± 200	3210 ± 280	0.0122 ± 0.0005	2480 ± 210	3317 ± 600

[a] The measured full width at half-maximum of the transient Doppler line widths for the translations $CO_2(00^00,J) \rightarrow CO_2(00^01, J-1)$, determined at 1 μs after DFB excitation in a 1:1 sample of DFB/CO_2 at a total pressure of 20 mTorr. The thermal Doppler line width for CO_2 at $T = 298$ K is $\Delta\nu_0 = 0.0042$ cm^{-1}. [b] The final translational temperature, T_{trans}, is obtained from fitting the experimentally determined Doppler line shapes with a Gaussian function and is related to the line width, $\Delta\nu_0$ (fwhm), through the expression $T_{trans}(K) = [mc^2(\Delta\nu_{obs})^2]/[8R \ln 2(\nu_0)^2]$, where m is the mass of CO_2, c is the speed of light, R is the gas constant, and ν_0 is the frequency at the center of the absorption line. [c] The final center of mass temperature, T_{trans}^{COM}, is obtained from the expression $T_{trans}^{COM}(K) = T_{trans} + (T_{trans} - T)(m_{CO_2}/m_{DFB})$, where T_{trans} is the temperature describing the CO_2 lab frame velocity, T is the ambient cell temperature, and m is the mass of CO_2 and difluorobenzene, respectively. [d] The internal energy of 1,2-DFB is $E' = 41\,025$ cm^{-1}, 1,3-DFB is $E' = 41\,011$ cm^{-1}, and 1,4-DFB is $E' = 41\,019$ cm^{-1}. [e] The final CO_2 rotational energy state following collision with vibrationally excited donor molecules.

TABLE 2: State-Specific Energy Transfer Rate Constants (k_2^J) and Probabilities[a] (k_2^J/k_{LJ}) for the Energy Transfer Process Difluorobenzene[E′] + $CO_2(00^00)$ → Difluorobenzene[E] + $CO_2(00^00,J,V)$

J_{final}	1,2-DFB	1,3-DFB	1,4-DFB
	k_2^J (10^{-12} cm^3 $molecule^{-1}$ s^{-1})		
58	6.6 ± 1.7	5.9 ± 1.3	6.4 ± 1.6
62	5.2 ± 1.3	3.7 ± 0.9	5.9 ± 1.5
66	2.7 ± 0.7	3.2 ± 0.8	3.6 ± 0.9
70	2.8 ± 0.7	2.2 ± 0.6	3.0 ± 0.7
72		1.8 ± 0.5	
76	1.8 ± 0.4	1.5 ± 0.4	2.2 ± 0.5
80	1.3 ± 0.3	1.4 ± 0.3	1.7 ± 0.4
	k_2^J/k_{LJ} (10^{-3})		
58	10.7 ± 2.7	9.60 ± 2.4	10.5 ± 2.6
62	8.4 ± 2.1	6.1 ± 1.5	9.7 ± 2.4
66	4.4 ± 1.1	5.2 ± 1.3	5.9 ± 1.5
70	4.5 ± 1.1	3.6 ± 0.9	4.7 ± 1.2
72		3.0 ± 0.8	
76	2.8 ± 0.7	2.5 ± 0.6	3.5 ± 0.9
80	2.1 ± 0.5	2.2 ± 0.6	2.8 ± 0.7

[a] The probability for energy transfer is given as $Prob_{LJ} = k_2^J/k_{LJ}$, where k_{LJ} is the Lennard-Jones has kinetic collision rate constant. It is defined (see ref 40) as $k_{LJ} = \pi[(d_{CO_2} + d_{DFB})/2]^2\sqrt{(8k_BT)/(\pi\mu)}\Omega_{12}$, where $d_{CO_2} = 4.5$ Å (ref 41), $d_{DFB} = 5.4$ Å (scaled relative to benzene, ref 41), k_B is Boltzmann's constant, and μ is the reduced mass. Ω_{12} is the Lennard-Jones collision integral given by the following expression:[36] $\Omega_{12} = [0.636 + 0.567 \log(k_BT/\epsilon_{12})]^{-1}$, where ϵ_{12} is the difluorobenzene−CO_2 well depth with $\epsilon_{CO_2}/k_B = 195$ K (ref 41), $\epsilon_{1,2-DFB}/k_B = 420$ K, $\epsilon_{1,3-DFB}/k_B = 408$ K, and $\epsilon_{1,4-DFB}/k_B = 416$ K (refs 42 and 43), and $\epsilon_{12} = \sqrt{\epsilon_{CO_2}\epsilon_{DFB}}$. The Lennard-Jones collision rate constants at 298 K for the three isomers of difluorobenzene are $k_{LJ(1,2-DFB)} = 6.17 \times 10^{-10}$, $k_{LJ(1,3-DFB)} = 6.13 \times 10^{-10}$, and $k_{LJ(1,4-DFB)} = 6.15 \times 10^{-10}$ cm^3 $molecule^{-1}$ s^{-1}.

by a room-temperature distribution. Previous work[9] has shown that use of an average initial rotational state introduces only a small amount of error for the high-J states; therefore, an average initial rotational state of $J_i = 28.7$ has been used for the $P(E,E')$ conversion process. Unlike the average initial J, the average initial relative velocity, also needed for the conversion process, can be determined using a translational gap law model.[6]

The energy transfer distribution function for single-collision relaxation of the three vibrationally excited DFB molecules by carbon dioxide is plotted in Figure 5. (Note that the probability is plotted versus $E - E'$ where E' is the donor precollision energy and E is the final donor energy.) A principle aspect of this work is to determine how molecular properties, in particular the frequency and character of the donor vibrational modes, affect the energy transfer probability distribution function. $P(E,E')$ for the three DFB/CO_2 systems can be compared not only to each other but also to $P(E,E')$ obtained in previous studies,[3,6,8−10] in particular hexafluorobenzene relaxation by CO_2.[3,7] To facilitate this comparison, $P(E,E')$ for C_6F_6 is also plotted in Figure 5. Because any comparison between $P(E,E')$ for different systems requires specification of both final and initial energies it is convenient to have one or two values to compare between the different systems; in other words, it is convenient to fit the experimentally obtained $P(E,E')$ to a model function.

The energy transfer distribution function shown in Figure 5 can be fit to either a single or a biexponential functional form. Single-exponential fits in the DFB systems provide an inaccurate fit to the experimental $P(E,E')$, as also seen in previous studies;[3,7,8] however, the biexponential model accurately fits the data, even when detailed balance and normalization are considered. The normalized, biexponential model, which has been used to include both strong and weak collisions, is given for down collisions according to[35]

$$P(E,E') = \frac{(1-f)\exp\{-(E'-E)/\alpha\} + f\exp\{-(E'-E)/\gamma\}}{(1-f)(\alpha+\beta) + f(\gamma+\delta)} \qquad E \le E' \quad (3)$$

In this model α is the average energy transfer for downward "weak" collisions, while γ is the average energy transfer for downward strong ("super") collisions. The up collision side of the model function is similar with the differences being the exchange of E and E' and the substitution of α and γ with β and δ, the respective average energy transfers for the upward "weak" and "strong" collisions. The up collision parameters are related to the down collision parameters by detailed balance.[36] The experimentally obtained energy transfer distribution function for the three DFB/CO_2 systems along with the best-fit, biexponential model function (eq 3) are shown in Figure 6, and the biexponential parameters with those from relaxation of C_6F_6 are summarized in Table 3.

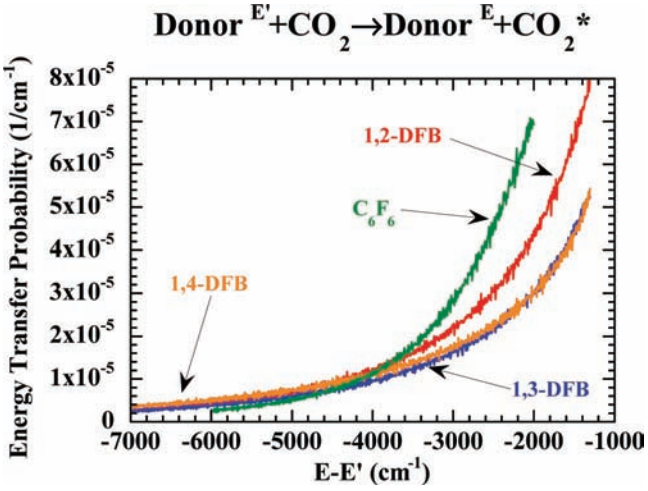

Figure 5. Plots of the large-ΔE tail of the energy transfer probability distribution function describing the first Lennard-Jones collision between a vibrationally excited DFB at energy $E' \approx 41\,000$ cm^{-1} and a CO_2 bath molecule resulting in excitation of the high CO_2 rotational angular momentum states ($J = 58-80$) of the ground vibrational level. E is the energy of the hot donor molecule following the collision. $P(E,E')$ for perfluorobenzne obtained from refs 3 and 7 is shown for comparison.

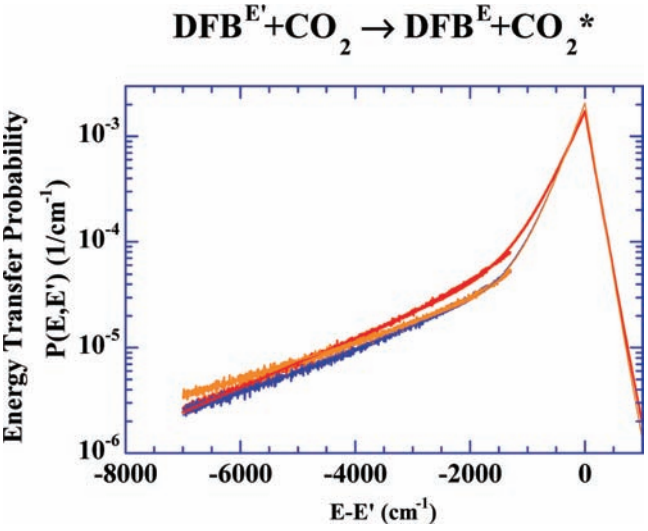

Figure 6. Plot of the energy transfer distribution function for the three DFB/CO_2 systems with $E' \approx 41\,000$ cm^{-1} (noisy line) along with the best-fit biexponential model functions (eq 3) (solid line). E is the energy of the hot donor molecule following the collision.

IV. Discussion

In previous studies involving collisions between carbon dioxide and vibrationally excited aromatic donor molecules, molecules scattered into the high angular momentum states of CO_2 arrive with large amounts of translational energy, determined by broad Doppler broadened line widths. In the case of collisions with the DFB isomers, the Doppler broadened line widths for the various J states are similar to each other within experimental error, as can be seen in Figure 4 and recorded in Table 1. A few exceptions include the line widths for $J = 58$ and 66 following collisions with 1,4-DFB, which are narrower than the CO_2 line widths for $J = 58$ and 66 following collisions with the other two isomers. In general the line widths increase linearly with final CO_2 rotational state, indicative of a constant impact parameter for these collisions in this range of final angular momentum states.[8] Although the line widths are similar in magnitude between the three isomers, CO_2 line widths following collisions with 1,4-DFB increase more over this range than the CO_2 line widths following collisions with the other two isomers. The CO_2 line widths following collisions with 1,2-DFB increase the least in this J state range.

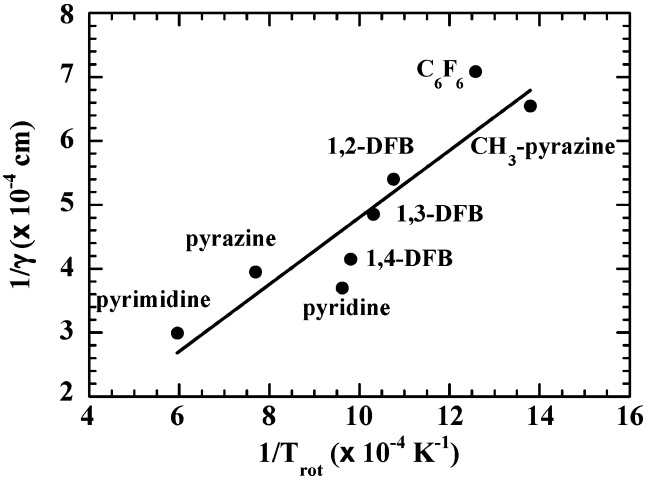

Figure 7. Comparison between the shape of the large ΔE tail of $P(E,E')$, characterized by $1/\gamma$, and the shape of the nascent postcollision CO_2 probability distribution, characterized by $1/T_{rot}$. T_{rot} is the rotational temperature that describes the population of the high-J states of CO_2 1 μs following laser excitation of donor molecules. The nearly one-to-one correspondence shows that the shape of $P(E,E')$ is determined almost entirely by final bath scattering probability.

Probabilities describing the scattering process are also similar for the three systems, with 1,4-DFB having slightly larger probabilities for scattering into the higher of the states probed in this study. The behavior of the energy transfer probabilities as a function of final CO_2 rotational state can be seen clearly in the Boltzmann plots in Figure 2. The rotational temperature that describes the high-J tail of the postcollision CO_2 distribution is the largest following collisions with 1,4-DFB (1040 K), followed by 1,3-DFB (970 K), and finally 1,2-DFB (930 K). The rotational temperature is a measure of the nascent CO_2 population in the high-J states and is, therefore, a convenient measure of the probability of exciting these high-J states during collisions with vibrationally excited donor molecules. As discussed elsewhere,[10] this rotational temperature is correlated with the shape of the energy transfer probability distribution function, $P(E,E')$. Figure 7 is a plot of the inverse of the exponential parameter that describes the large ΔE region of $P(E,E')$, $1/\gamma$, for a series of donor/CO_2 systems studied to date at 248 nm versus the inverse of the rotational temperature that describes scattering into the high CO_2 rotational states, $1/T_{rot}$. As can be seen, the correlation between rotational temperature and the shape of the large ΔE region of $P(E,E')$ is very high. The high correlation is expected because there are only a few other factors involved in the conversion of state-resolved data into $P(E,E')$. These factors include the final center of mass translational temperatures and the magnitudes of the probabilities. In the case of C_6F_6, deviation seen in Figure 7 is likely due to the way CO_2 line widths following collisions with C_6F_6 vary with J. Line widths are essentially constant for $J = 58-76$ and then increase dramatically for the remaining J states probed.[7] In the case of 1,4-DFB, the deviation may also relate to the way the final center of mass translational temperatures vary with the final CO_2 J state. As noted above, the CO_2 line widths (and T_{COM}) increase more over this range of final rotational states than the other DFB systems studied. For pyridine, the deviation in Figure 7 may be related to the very low probability for scattering into these states.[10] Clearly the

TABLE 3: Energy Transfer Probability Distribution Function Double-Exponential Fit Parameters (the Characteristic Energy Transfer Frequencies for Both Strong and Weak Down Collisions, the Fraction of Strong Collisions, and the Average Down Collision Energy) as Well as Several Donor Molecular Properties (Dipole Moment, Donor Density of States, and the Number of Low-Frequency Vibrational Modes)

	γ^a (cm^{-1})	α^b (cm^{-1})	f^c	$\langle\Delta E\rangle_d{}^d$ (cm^{-1})	dipole moment[e] (D)	$\rho(E')^f$	$s < 500\ cm^{-1}$ [g]
C_6F_6[h]	1411	620	0.15	847	0	2.1×10^{23}	13
1,2-DFB	1850	343	0.06	739	2.59	5.7×10^{17}	5
1,3-DFB	2061	295	0.03	638	1.51	5.2×10^{17}	5
1,4-DFB	2408	294	0.03	713	0	5.5×10^{17}	6

[a] The characteristic strong energy transfer magnitude as determined from the biexponential fit of the $P(E,E')$ data. [b] The characteristic weak energy transfer magnitude as determined from the biexponential fit of the $P(E,E')$ data. [c] The "fraction" of strong collisions as determined from the biexponential fit of the $P(E,E')$ data. [d] The average energy transferred in a single downward collision involving a vibrationally excited donor and CO_2. Determined using the biexponential fit parameters according to $\langle\Delta E\rangle_d = (\alpha^2(1-x) + \gamma^2 x)/(\alpha(1-x) + \gamma x)$. [e] Molecular dipole moment obtained from ref 44. [f] The vibrational density of states for the donor molecule at the energy following the absorption of a 248 nm photon calculated using the Whitten−Rabinovitch algorithm (ref 45). [h] The number of vibrational normal modes with frequencies less than 500 cm^{-1}. Normal-mode frequencies for C_6F_6 and 1,2-, 1,3-, and 1,4-DFB are obtained from refs 46 and 47, 48 and 49, 19 and 48, and 48 and 50, respectively. [h] $P(E,E')$ parameters obtained from ref 3.

shape of the large ΔE tail of $P(E,E')$ is generally correlated with the rotational temperature describing the high-J postcollision bath states; however, deviations can occur due to other factors used to construct $P(E,E')$ from state-resolved data.

A principle aspect of our research is to understand the molecular properties of the donors involved in collisional energy transfer processes that govern the shape of $P(E,E')$. Table 3 contains the biexponential fit parameters, obtained by fitting the experimentally measured $P(E,E')$ to eq 3, as well as values for several molecular properties: density of states, number of low-frequency vibrational modes, and dipole moment. Results of previous studies[10] seemed to suggest that the fraction of strong collisions was correlated with the number of low-frequency donor modes, with more low-frequency modes resulting in a greater "fraction" of strong collisions. However, a comparison of the "fraction" of strong collisions to the number of donor vibrational modes with a frequency $<500\ cm^{-1}$ listed in Table 3 shows that these two factors do not appear to be correlated. For the DFBs, even though 1,4-DFB has the most vibrational modes with frequencies $<500\ cm^{-1}$, it has the smallest value of f. The correlation observed between the number of low-frequency modes and f for other systems may have just been fortuitous, or this may be a result of using too simple a model and the arbitrariness of determining what constitutes "low-frequency" motion.

Alternatively, the fraction of strong collisions could be related to the dipole moment of the donor molecule, as suggested by energy transfer studies of pyridine.[10] Work by Mullin and coworkers[17] showed that pyridine has an enhanced $V \rightarrow V$ energy transfer channel relative to the $V \rightarrow RT$ channel when compared with energy transfer from pyrazine. They concluded that this was a result of pyridine's large, 2.2 D, dipole moment. Studies in our lab indicated that $P(E,E')$ for pyridine has only a small "fraction" of strong collisions compared to other donor molecules, $f = 0.008$. We concluded that the large dipole moment of pyridine, which caused enhanced $V \rightarrow V$ energy transfer and relatively decreased $V \rightarrow RT$ energy transfer, led to a smaller $P(E,E')$ strong collision tail. One reason for these studies was to measure $P(E,E')$ resulting from the collisional deactivation of similar molecules with different dipole moments. However, as can be seen in Table 3, the effects are not what we had predicted based on the pyridine studies. 1,2-DFB with the largest dipole moment also has the largest fraction of strong collisions of the three DFBs, while 1,3- and 1,4-DFB have similar fractions of strong collisions. Therefore it appears that dipole moment is not a direct measure of the "fraction" of strong collisions. Studies of $V \rightarrow V$ are needed to confirm the affect of dipole moment on energy transfer for these systems. It may also be that these studies have exposed one of the greatest limitations of the diode laser method to measuring $P(E,E')$, the current limitation of measuring only the large ΔE region, a limitation that we are working to eliminate.

In contrast to these molecular properties that do not seem to have a simple correlation with the $P(E,E')$ parameters, there appears to be a correlation between the $P(E,E')$ parameters and the donor density of states. Increasing strong collision energy, γ, is generally correlated in these studies with decreasing weak collision energy, "fraction" of strong collisions, average energy transferred in down collisions, and donor density of states. On the basis of these correlations, it appears that the initial donor density of states is associated with the factors that describe the shape of $P(E,E')$. As has been seen in previous studies in both our lab[9,10] and the Mullin lab,[11−14] correlation exists between the shape of $P(E,E')$ and the way that the donor molecule final density of states changes with internal energy. This model, based on Fermi's Golden Rule, is given according to

$$P(E,E') \propto |V_{if}|^2 \rho(E)\rho(E') \tag{4}$$

where $\rho(E)$ is the density of states at energy E and V_{if} is the matrix element, $\langle i|H|f\rangle$, that couples the initial and the final states. Figure 8 shows a plot of the inverse of the characteristic energy transfer energies (the "slope" of $P(E,E')$) obtained by fitting $P(E,E')$ to eq 3 as a function of the slope obtained from plotting $\ln[\rho(E' - \Delta E)]$ versus ΔE[13] for the relaxation of pyrazine,[6] C_6F_6,[7]methylpyrazine,[8] pyrimidine,[9] pyridine,[10] and the three DFB isomers each with $E' \approx 41\ 000\ cm^{-1}$ by collisions with CO_2. As can be seen in Figure 8, the inverses of both the strong and the weak characteristic energy transfer magnitudes are linearly related to the slope of $\ln[\rho(E' - \Delta E)]$ versus ΔE. The correlation between the energy-dependent density of states and the strong collision parameter, shown in Figure 8 by the circles, is very good, while the correlation with the weak collision energy, shown by the squares, is only generally good. This is not a surprising result, given that the tail of $P(E,E')$, described by the strong collision energy, is well-defined in these experiments, while the small ΔE portion of $P(E,E')$ reported here is the result of an extrapolation of the data according to eq 3. That said, the extrapolated values of the weak collision energy are within 20% of the value of the best-fit line; this is approximately the same error as associated with the experimentally measured energy transfer rate constants.

The correlation between $P(E,E')$ shape and the energy dependence of the donor density of states is satisfying; however,

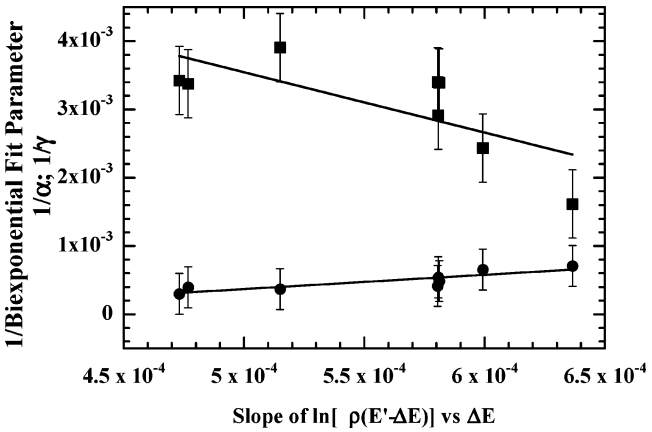

Figure 8. Correlation between the shape of $P(E,E')$ as determined by the biexponential fit parameters ($1/\alpha$ and $1/\gamma$) and the energy-dependent state density of the donor molecules on the basis of the application of Fermi's Golden Rule to collisional deactivation of vibrationally excited donor molecules in collisions with CO_2. Circles represent the characteristic energy transfer magnitudes for "strong" collisions (γ) while the squares are the characteristic energy transfer magnitudes for "weak" collisions (α) From left to right in the figure, data points are for pyrimidine, pyrazine, pyridine, the three DFB isomers, methylpyrazine, and C_6F_6. Pyrazine, C_6F_6, methylpyrazine, pyrimidine, and pyridine data are from refs 3 and 7−10. The shape of the energy transfer distribution function as a function of ΔE mirrors the shape of the final donor density of states as a function of energy transferred (ΔE). The shape of both the strong and the weak collision region of $P(E,E')$ is correlated with the donor molecule's final density of states.

it is potentially misleading in terms of how energy transfer in these systems occurs at the molecular level. At first blush, one might assume that stiff, high-frequency donor vibrational modes are responsible for large energy transfer events, because the molecules with the most high-frequency modes have the largest strong collision energy; however, a more careful look at the nature of eq 4 and the data in Figure 8 should lead one to the opposite conclusion. Low-frequency modes have the greatest influence on how the density of states changes with internal energy. The more low-frequency modes a molecule has, the larger the magnitude of the slope of $\ln[\rho(E' - \Delta E)]$ versus ΔE, which is correlated with the shape of $P(E,E')$. Thus it is low-frequency molecular motion, not high-frequency motion, that controls the shape of the large ΔE tail of the energy transfer distribution function. This observation is consistent with other experimental and computation evidence, indicating that low-frequency donor modes have primary control over the shape of $P(E,E')$.

Both quantum scattering and classical trajectory studies[15,16] indicate that low-frequency donor vibrational modes have the largest cross-sections for transferring large amounts of energy in a single event. Of particular relevance to our studies of energy transfer from the DFB isomers is the quantum scattering study[15] of benzene relaxation by collisions with He. Clary et al. observed that in this relaxation process only three of the benzene modes had significant energy transfer cross-sections, ν_6, ν_{11}, and ν_{16}, with ν_{16}, the lowest-frequency mode, being the most efficient at transferring energy. These computational studies further indicated that in addition to mode frequency the motion of the mode was also an important factor in determining the magnitudes of the cross-sections for large energy transfer. Even when ν_6, a higher-frequency stretching mode, was artificially altered to have the same frequency as ν_{16}, an out-of-plane mode, ν_{16} still had a greater energy transfer cross-section for large energy transfer events. Lendvay[16] has called these efficient energy transfer vibrational modes gateway modes, referring to them as conduits through which energy can efficiently leak out of the donor into the bath.

TABLE 4: Vibrational Mode Assignments and Frequencies (in cm^{-1}) for Out-of-Plane[a] and Gateway[b] Modes for the Three DFB Isomers and Hexafluorobenzene

vibrational mode[c]	1,2-DFB[d]	1,3-DFB[e]	1,4-DFB[f]	C_6F_6[g]
4-o	704	673	692	249
6a-g	570	523	450.4	370
6b-g	538.5	514	635	370
10a-o	275	250.5	800	370
10b-o	198	230	374.5	370
11-o/g	749	770	161.75	210
16a-o/g	574	601	421.5	120
16b-o/g	450	458	504.5	120
17a-o	845	879	944	595
17b-o	929	850	835.5	595

[a] Out-of-plane modes have been labeled with o. [b] Gateway modes have been labeled with g. [c] The vibrational frequencies are labeled according to Wilson notation; see ref 37. [d] Vibrational frequencies obtained from refs 48 and 49. [e] Vibrational frequencies obtained from refs 19 and 48. [f] Vibrational frequencies obtained from refs 48 and 50. [g] Vibrational frequencies obtained from refs 46 and 47.

The gateway mode concept is further supported by experimental results. We have presented a "fractional energy transfer distribution model"[8−10] that takes into account both the efficiency of the mode and the fraction of molecules with enough energy in that mode to transfer a given amount of energy. Our model indicates that low-frequency donor gateway vibrational modes control the shape of the large ΔE tail of $P(E,E')$. Because our model only allows one to compare modes with the same molecular motion, one limitation of our previous use of this model has been comparing donors with different numbers of vibrational modes. A primary aspect of this study of energy transfer from the three DFB isomers to CO_2 is to compare $P(E,E')$ between donors with the same number of vibrational modes (each with the same motion) but that have different frequencies depending on the position of the fluorine atoms. The purpose is to see if experimentally obtained $P(E,E')$ values are consistent with the gateway mode concept and to determine if an understanding of the various donor modes can aid in deducing the shape and magnitude of $P(E,E')$.

Table 4 contains a list of some of the vibrational modes of the three DFB isomers and hexafluorobenzene along with their frequencies. The vibrational modes listed correspond either to the gateway modes observed in the quantum scattering calculations, discussed above, or to the remaining donor molecule out-of-plane modes for comparison. Out-of-plane modes were included because they generally have lower frequencies, which have been linked to larger energy transfer cross-sections. Modes are listed using Wilson notation,[37,38] which is an assignment linked to the vibrational motion and not necessarily the symmetry or frequency. Thus ν_1 has the same motion for each molecule, regardless of the point group of the molecule or the frequency of the mode relative to the remaining modes of the same symmetry. Comparing C_6F_6 to the three DFB isomers, C_6F_6 typically has the lowest frequency for all of the modes listed. Considering the computational work, this should indicate that C_6F_6 is a more efficient energy transfer donor; however, the efficiency of a mode at transferring a large amount of energy is only part of the picture.[8−10] In addition to efficiency, one must consider the fraction of molecules in that vibrational mode with enough energy to affect the energy transfer magnitude in question. In other words, if one is considering the probability of transferring 2000 cm^{-1} and the energy transfer leaks out

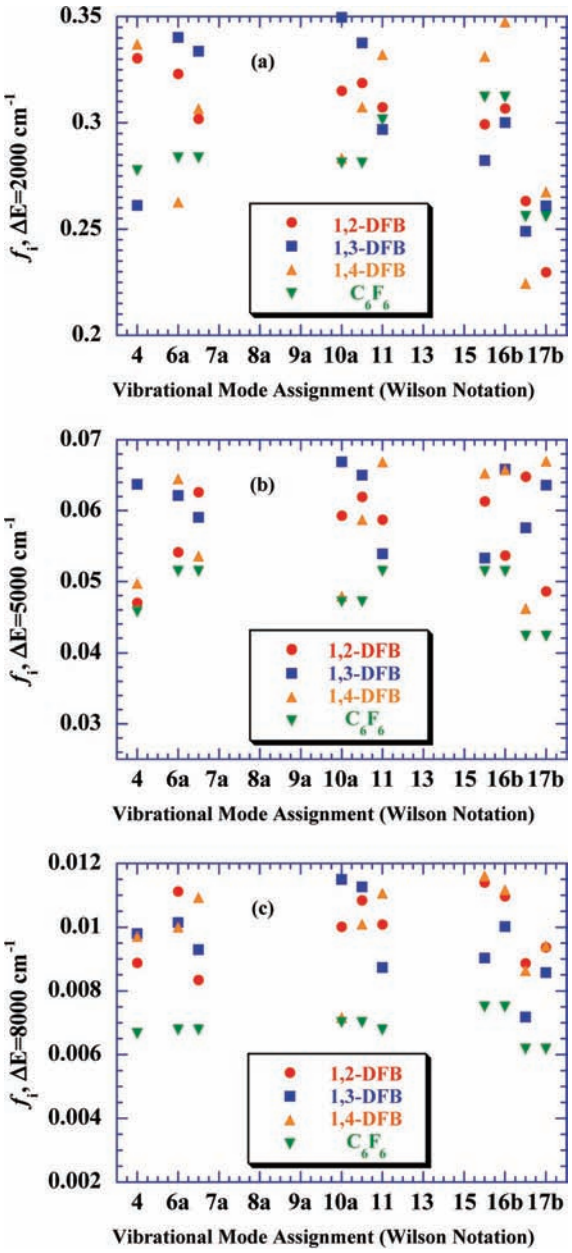

Figure 9. Fractional mode populations for highly vibrationally excited ($E' \approx 41\,000$ cm^{-1}) 1,2-, 1,3-, and 1,4-DFB and C_6F_6 with at least (a) 2000, (b) 5000, and (c) 8000 cm^{-1}. The *x*-axis is the vibrational mode assignment according to Wilson notation, which has been used so that mode assignments represent the same vibrational motion in each molecule. Only the vibrational modes that were determined to be gateway energy transfer modes in the quantum scattering calculation (ref 15) of the relaxation of benzene by He (ν_{6a}, ν_{6b}, ν_{11}, ν_{16a}, and ν_{16b}) and the remaining out-of-plane vibrational modes (ν_4, ν_5, ν_{10a}, ν_{10b}, ν_{17a}, and ν_{16b}) are included. C_6F_6 has the smallest fraction of molecules in every mode at all energies, except for ν_{16a} and ν_{16b} at 2000 cm^{-1}, where it has the second largest population. C_6F_6 has the largest energy transfer probability at 2000 cm^{-1}, but the smallest at 5000 and 8000 cm^{-1}, as seen in Figure 5. The correlation between fractional mode populations of ν_{16a} and ν_{16b} and $P(E,E')$ suggests that this mode is one that governs $P(E,E')$ shape. The vibrational frequencies for the three DFB isomers are similar for most modes, with the exception of ν_{11} and ν_{10a}. A comparison of the fractional mode populations of these modes for the three DFB molecules indicates that the fraction of molecules with sufficient energy to transfer 2000, 5000, and 8000 cm^{-1} from ν_{11} is the largest for 1,4-DFB while the fractions in ν_{10a} are the largest for 1,2- and 1,3-DFB. Comparison to experimental $P(E,E')$ indicates that 1,4-DFB produces the largest energy transfer probability in the tail of the distribution, supporting ν_{11} as a gateway mode that governs $P(E,E')$ shape.

through a certain mode, then we need to know the fraction of donor molecules that have at least 2000 cm^{-1} in that mode. This fraction can be calculated according to[39]

$$f_i = \frac{\sum_{\upsilon=\min}^{\max} \rho_{s-1}(E - \upsilon h\nu_i)}{\rho_s(E)} \quad (5)$$

where $\rho_s(E)$ is the density of states for all *s* oscillators at energy *E* and $\rho_{s-1}(E - \upsilon_i h\nu_i)$ is the density of states for all *s* oscillators at energy *E* and the densities of states for all oscillators except the mode of interest at an energy of $E - \upsilon h\nu_i$. ν_i is the frequency of the mode of interest, and υ is the vibrational quantum number of that mode. $\upsilon = \max$ corresponds to the maximum possible value of the vibrational quantum number of that mode, given according to $\max = E/h\nu_i$. $\upsilon = \min$ corresponds to the lowest vibrational quantum number necessary to populate the mode of interest with the minimum amount of energy necessary for a certain energy transfer, ΔE, and is found according to $\min = \Delta E/h\nu_i$. For example, if $\nu_i = 315$ cm^{-1}, the total energy of the molecule is 41 000 cm^{-1}, and the amount of energy transfer is 2000 cm^{-1}, then $\upsilon_{max} = 130$ and $\upsilon_{min} = 7$. Notice that the total density of states is the denominator of eq 5; thus, molecules with large state densities have smaller fractions populating their modes than do molecules with smaller state densities, even when considering the same mode with similar frequencies in different molecules.

Figure 9 displays the fractional mode populations for 1,2-, 1,3-, and 1,4-DFB and C_6F_6 with at least (a) 2000, (b) 5000, or (c) 8000 cm^{-1} of energy in the mode. The *x*-axis is the Wilson assignment of the mode, and only the vibrational modes listed in Table 4 have been plotted. Looking only at Figure 9a, C_6F_6 has the smallest or nearly the smallest fraction of molecules with at least 2000 cm^{-1} in most modes considered. The lone exception is ν_{16} in which C_6F_6 has the second largest fraction of molecules. When considering the fraction of molecules with at least 5000 (Figure 5b) or 8000 cm^{-1} (Figure 5c), C_6F_6 has the smallest fraction of molecules with that energy for all modes considered. Thus, even though its vibrational modes have a lower frequency and, according to quantum scattering and classical trajectory calculations, a greater energy transfer efficiency, the fraction of molecules with at least 5000 or 8000 cm^{-1}, the energy necessary to scatter CO_2 into high-*J* states, is smaller than those in the DFB molecules; therefore, the large ΔE tail of $P(E,E')$ for C_6F_6/CO_2 collisions should have a smaller probability than the DFB molecules, which it does, as seen experimentally in Figure 5. In other words, the average energy in the low-frequency modes of C_6F_6 is smaller than those for the DFBs; therefore, despite being more efficient, the low-frequency modes do not have as much energy to transfer. At 2000 cm^{-1}, the energy transfer probability is different than that at 5000 or 8000 cm^{-1}. At 2000 cm^{-1}, C_6F_6 has a large experimentally determined energy transfer probability as seen Figure 5. This is the result of energy leaking out of a mode that is both efficient and populated with sufficient energy to produce the large experimentally observed energy transfer probability. ν_{16} is the only mode that satisfies these criteria, having a low frequency, which suggests high efficiency, and a relatively large population. Additionally, because the fraction of molecules with at least 5000 and 8000 cm^{-1} in this mode decreases in a way that mirrors how $P(E,E')$ decreases with increasing ΔE, this mode appears to be the dominate energy transfer gateway for energy transfer from C_6F_6 to CO_2.

Considering the vibrational frequencies of the three DFB isomers, two modes stand out as different between the three

molecules. The frequency of ν_{11} for 1,4-DFB is ~80% lower than the frequency of the other two DFBs. On the basis of the quantum scattering and trajectory studies, this mode, in 1,4-DFB, should be a more efficient energy transfer donor than the same motion in the other two isomers. On the basis of the data in Figure 9 for 1,4-DFB, ν_{11} has a larger fraction of molecules than the same mode in the other donors. This is true at all three values of ΔE, but the fraction of molecules in ν_{11} for 1,4-DFB is greater relative to those of the other two isomers at the larger ΔE values. On the basis of this greater fraction of molecules with sufficient energy to transfer 2000, 5000, or 8000 cm^{-1} and this more efficient gateway (as determined by lower frequency), one might expect the energy transfer probability for large energy transfers to be greater for 1,4-DFB than those for the other two isomers. In contrast to this, the frequency of ν_{10a} for 1,4-DFB is ~70% greater than those for the other two donors, and the fraction of 1,4-DFB molecules with 2000, 5000, and 8000 cm^{-1} in ν_{10a} is less than those for the other isomers, which would suggest just the opposite effect, and lead one to the conclusion that 1,2- and 1,3-DFB would have greater probabilities for transferring large amounts of energy in a single collision. An examination of $P(E,E')$ for the three donors, shown in Figure 5, shows that at 2000 cm^{-1} 1,2-DFB has the greatest energy transfer probability with 1,3-DFB and 1,4-DFB smaller but similar to each other. By 5000 cm^{-1}, 1,4-DFB has a larger energy transfer probability than those of the other two DFB donors. The experimentally observed $P(E,E')$ values are consistent with energy transfer from ν_{11} when considering the three DFB isomers.

$P(E,E')$ values obtained in these studies and compared to $P(E,E')$ for C_6F_6 obtained previously are consistent with the concept of energy leaking out of only a few vibrational modes of the donor, in this case ν_{11} and ν_{16}. These are two of the donor vibrational modes that Clary et al.[15] determined to have large energy transfer efficiencies. Thus, energy transfer from the three vibrationally excited DFB isomers is consistent with previous studies, both experimental and theoretical, which related donor mode character, frequency, and energy-dependent density of states. The application of Fermi's Golden Rule to the study of relaxation of highly vibrationally excited molecules indicates that the shape of $P(E,E')$ is related to how the donor molecule's density of states changes with internal energy. Because this model has been successful at accurately describing the shape of $P(E,E')$, eventually this may provide a means to predict the $P(E,E')$ for unmeasured systems. Experimental evidence of a microscopic picture of energy transfer from gateway modes is also starting to develop. In these studies, the experimental energy transfer probability is consistent with energy leaking out of ν_{11} and ν_{16}, also observed in quantum scattering calculations of energy transfer from benzene to He.[15]

V. Conclusion

The relaxation of highly vibrationally excited 1,2-, 1,3-, and 1,4-DFB by collisions with a bath of carbon dioxide has been studied using infrared diode laser spectroscopy to probe scattered bath molecules. The nascent rotational populations and recoil velocity distributions for rotational states in the high-J tail ($J = 58-80$) of the 00^00 level of CO_2 were measured. The recoil velocity distributions indicate that significant translational excitation accompanies the rotational excitation of bath molecules scattered into high-J states of the ground vibrational level. State-indexed energy transfer probabilities have been resorted as a function of ΔE to extract the large ΔE tail of the energy transfer distribution function, $P(E,E')$. $P(E,E')$ has been fit to a double-exponential model form for comparison to previous experiments. The rotational temperature describing the high-J tail of the nascent CO_2 distribution for all donors studied is strongly correlated with the biexponential fit parameter that describes the large ΔE tail of $P(E,E')$. The fit parameters that describe both the large ΔE portion of $P(E,E')$ (strong collision energy) and the small ΔE portion of $P(E,E')$ (weak collision energy) are related to how the donor molecule density of states changes as a function of internal energy. Finally, comparisons of fractional mode populations in donor vibrational modes that computational studies have suggested are gateway modes for energy transfer suggest that two modes, ν_{11} and ν_{16}, are the dominant contributors to the shape of $P(E,E')$ for energy transfer from C_6F_6 and the three DFB isomers.

Acknowledgment. This work was performed at Brigham Young University with support from the BYU Mentoring Environment Grant. J.A.J. acknowledges support from the BYU Office of Research and Creative Activities Fellowship program. J.A.J., K.A.J., M.M., D.G.M., and A.J.P. acknowledge support from the Department of Chemistry and Biochemistry Undergraduate Research Awards program.

References and Notes

(1) Levine, R. D. *Molecular Reaction Dynamics*; Cambridge University Press: Cambridge, U. K., 2005.
(2) Gilbert, R. G.; Smith, S. C. *Theory of Unimolecular and Recombination Reactions*; Blackwell Scientific Publications: Oxford, U. K., 1990.
(3) Michaels, C. A.; Flynn, G. W. *J. Chem. Phys.* **1997**, *106*, 3558.
(4) Hold, U.; Lenzer, T.; Luther, K.; Reihs, K.; Symonds, A. C. *J. Chem. Phys.* **2000**, *112*, 4076.
(5) Liu, C.-L.; Hsu, Hsu, C.; Lyu, J.-J.; Ni, C.-K. *J. Chem. Phys.* **2005**, *123*, 131102.
(6) Mullin, A. S.; Michaels, C. A.; Flynn, G. W. *J. Chem. Phys.* **1995**, *102*, 6032.
(7) Michaels, C. A.; Lin, Z.; Mullin, A. S.; Tapalian, H. C.; Flynn, G. W. *J. Chem. Phys.* **1996**, *106*, 7055.
(8) Sevy, E. T.; Rubin, S. M.; Lin, Z.; Flynn, G. W. *J. Chem. Phys.* **2000**, *113*, 4912.
(9) Johnson, J. A.; Duffin, A. M.; Hom, B. J.; Jackson, K. E.; Sevy, E. T. *J. Chem. Phys.* **2008**, in press.
(10) Johnson, J. A.; Kim, K.; Mayhew, M.; Mitchell, D. G.; Sevy, E. T. *J. Phys. Chem. A* **2008**, in press.
(11) Miller, E. M.; Murat, L.; Bennette, N.; Hayes, M.; Mullin, A. S. *J. Phys. Chem. A* **2006**, *110*, 3266.
(12) Park, J.; Li, Z.; Lemoff, A. S.; Rossi, C.; Elioff, M. S.; Mullin, A. S. *J. Phys. Chem. A* **2002**, *106*, 3642.
(13) Park, J.; Shum, L.; Lemoff, A. S.; Werner, K.; Mullin, A. S. *J. Chem. Phys.* **2002**, *117*, 5221.
(14) Elioff, M. S.; Fang, M.; Mullin, A. S. *J. Chem. Phys.* **2001**, *115*, 6990.
(15) Clary, D. C.; Gilbert, R. G.; Bernshtein, V.; Oref, I. *Faraday Discuss.* **1995**, *102*, 423.
(16) Lendvay, G. *J. Phys. Chem. A* **1997**, *101*, 9217.
(17) Wall, M. C.; Stewart, B. A.; Mullin, A. S. *J. Chem. Phys.* **1998**, *108*, 6185.
(18) Cooper, C. D. *J. Chem. Phys.* **1954**, *22*, 503.
(19) Graham, P. A.; Kable, S. H. *J. Chem. Phys.* **1995**, *103*, 6426.
(20) Tsuchiya, Y.; Takazawa, K.; Fujii, M.; Ito, M. *Chem. Phys. Lett.* **1991**, *183*, 107.
(21) Volk, L. J.; Lee, E. K. C. *J. Chem. Phys.* **1977**, *67*, 236.
(22) Guttman, C.; Rice, S. A. *J. Chem. Phys.* **1974**, *61*, 661.
(23) Khan, F. A.; Kreutz, T. G.; Flynn, G. W.; Weston, R. E., Jr. *J. Chem. Phys.* **1990**, *92*, 4876.
(24) Parker, G. A.; Pack, R. T. *J. Chem. Phys.* **1978**, *68*, 1585.
(25) Abrams, R. L.; Cheo, P. K. *Appl. Phys. Lett.* **1969**, *15*, 177.
(26) Agrawal, P. M.; Raff, L. M. *J. Chem. Phys.* **1981**, *75*, 2163.
(27) Brownsword, R. A.; Salh, J. S.; Smith, I. W. M. *J. Chem. Soc., Faraday Trans.* **1995**, *91*, 191.
(28) Pack, R. T. *J. Chem. Phys.* **1979**, *70*, 3424.
(29) Roche, C.; Millot, G.; Chaux, R.; Saint-Loup, R. *J. Chem. Phys.* **1994**, *101*, 2863.
(30) Hershberger, J. F.; Chou, J. Z.; Flynn, G. W.; Weston, R. E., Jr. *Chem. Phys. Lett.* **1988**, *149*, 51.
(31) Michaels, C. A.; Mullin, A. S.; Flynn, G. W. *J. Chem. Phys.* **1995**, *102*, 6682.

(32) Sedlacek, A. J.; Weston, R. E., Jr.; Flynn, G. W. *J. Chem. Phys.* **1991**, *94*, 6483.
(33) Pugh, L. A.; Rao, K. N. Intensities from infrared spectra. In *Molecular Spectroscopy: Modern Research*; Rao, K. N., Ed.; Academic Press: New York, 1976; Vol. II, p 165.
(34) Rothman, L. S.; Gamache, R. R.; Barbe, A.; Goldman, A.; Gillis, J. R.; Brown, L. R.; Toth, R. A.; Flaud, J. M.; Camy-Peyret, C. *Appl. Opt.* **1983**, *22*, 2247.
(35) Troe, J. *J. Chem. Phys.* **1992**, *97*, 288.
(36) Troe, J. *J. Chem. Phys.* **1977**, *66*, 4758.
(37) Wilson, E. B., Jr. *Phys. Rev.* **1934**, *45*, 706.
(38) Lord, R. C.; Marston, A. L.; Miller, F. A. *Spectrochim. Acta* **1957**, *9*, 113.
(39) Durana, J. F.; McDonald, J. D. *J. Chem. Phys.* **1976**, *64*, 2518.
(40) Smith, I. W. M. *Kinetics and Dynamics of Elementary Gas Reactions*; Butterworths: London, 1980.
(41) Hirschfelder, J. O.; Curtiss, C. F.; Bird, R. B. *Molecular Theory of Gases and Liquids*; John Wiley & Sons: New York, 1954.
(42) Kable, S. H.; Thoman, J. W., Jr.; Knight, A. E. W. *J. Chem. Phys.* **1988**, *88*, 4748.
(43) Lawrence, W. D.; Knight, A. E. W. *J. Chem. Phys.* **1983**, *79*, 6030.
(44) Doraiswamy, S.; Sharma, S. D. *J. Mol. Struct.: THEOCHEM* **1983**, *94*, 63.
(45) Whitten, G. Z.; Rabinovitch, B. S. *J. Chem. Phys.* **1963**, *38*, 2466.
(46) Eaton, V. J.; Steele, D. *J. Mol. Spectrosc.* **1973**, *48*, 446.
(47) Pearce, R. A. R.; Steele, D.; Radcliffe, K. *J. Mol. Struct.* **1973**, *15*, 409.
(48) Kwon, C. H.; Kim, H. L.; Kim, M. S. *J. Chem. Phys.* **2003**, *118*, 6327.
(49) Lunelli, B.; Giorgini, M. G. *J. Mol. Spectrosc.* **1977**, *64*, 1.
(50) Elston, H. J.; Davidson, E. R.; Todd, F. G.; Parmenter, C. S. *J. Phys. Chem.* **1993**, *97*, 5506.